LA-UR- 10-03330

Approved for public release; distribution is unlimited.

Title: Phase-Contrast Imaging Using Ultrafast X-Rays in Shocked Materials

Author(s): Jonathan B Workman, James A Cobble, Kirk Flippo, D. Cort Gautier, David S. Montgomery, Dustin T Offermann P-24

Intended for: 19th Topical Conference on High-Temperature Plasma Diagnostics
Wildwood, NJ
May 16-20, 2010

Los Alamos
NATIONAL LABORATORY
EST. 1943

Phase-Contrast Imaging Using Ultrafast X-Rays in Laser-Shocked Materials[a)]

J. Workman,[1,b)] J. Cobble,[1] K. Flippo,[1] D.C. Gautier,[1] D.S. Montgomery,[1] D. Offermann[1]

[1]*Los Alamos National Laboratory, Los Alamos NM 87545 USA*

(Presented XXXXX; received XXXXX; accepted XXXXX; published online XXXXX)

High-energy x-rays, >10-keV, can be efficiently produced from ultrafast laser target interactions with many applications to dense target materials in Inertial Confinement Fusion (ICF) and High-Energy Density Physics (HEDP). These same x-rays can also be applied to measurements of low-density materials inside high-density hohlraum environments. In the experiments presented, high-energy x-ray images of laser-shocked polystyrene are produced through phase contrast imaging. The plastic targets are nominally transparent to traditional x-ray absorption but show detailed features in regions of high density gradients due to refractive effects often called phase contrast imaging. The 200-TW Trident laser is used both to produce the x-ray source and to shock the polystyrene target. X-rays at 17-keV produced from 2-ps, 100-J laser interactions with a 12-micron molybdenum wire are used to produce a small source size, required for optimizing refractive effects. Shocks are driven in the 1-mm thick polystyrene target using 2-ns, 250-J, 532-nm laser drive with phase plates. X-ray images of shocks compare well to 1-D hydro calculations, HELIOS-CR.

I. INTRODUCTION

High-energy x-ray generation from ultrafast lasers has been developed over the past several years for applications in Inertial Confinement Fusion (ICF) and High-Energy Density Physics (HEDP)[123]. X-ray line emission from ultrafast laser target interactions generally exceed the conversion efficiency from thermal nanosecond laser interactions when applied to x-ray energies >10-keV. The interaction of an ultrafast laser produces large electric fields that accelerate electrons to energies as high as 100-MeV[4] with conversion of laser energy into electron energy of order 10-30%. Electrical currents that setup in the target allow the electrons to oscillate producing collisions in the cold and warm regions of the target with the emission of Kα x-rays, much like a traditional x-ray tube. While the desire to extend laser–driven x-ray sources to higher x-ray energies is driven primarily by new higher areal density experiments proposed on NIF, OMEGA-EP and ZR there is also a need to look through high-Z hohlraum walls at eg. shocks and interface motion in foams, plastics and other lower-Z materials. In order to accomplish this we rely on phase contrast imaging. This technique takes advantage of the real part of the index of refraction for x-rays and tries to minimize the imaginary part, known traditionally as absorption. For example, to minimize x-ray absorption in a 10-μm gold hohlraum wall requires x-ray energies above 30-keV. X-rays produced under the right geometric conditions will produce an interference pattern in the region of high density gradients, typically defined as an interface. While there has been significant recent work using phase contrast imaging for static characterization[5678] there are significant challenges to using this technique in a dynamic environment.

This article describes experiments conducted on the 200-TW Trident laser facility in Los Alamos, NM to demonstrate phase contrast imaging using ultrafast laser-produced x-rays at high x-ray energies to observe nanosecond laser-generated shocks in a polystyrene target. The results from the phase contrast image are compared to calculations. The results from these experiments will be used to scale experiments to NIF.

II. EXPERIMENTAL CONFIGURATION

Experiments were performed at the 200-TW Trident Laser Facility using both the ultrafast laser and nanosecond laser capabilities to drive the backlighter target and drive a shock into a polystyrene target. Backlighters consisted of 12.5-μm diameter molybdenum wires of length 300-μm mounted on plastic or aluminum substrates and held by a glass stalk. Polystyrene targets consisted of 2-mm diameter disks with thickness 1-mm. The polystyrene disks were irradiated face-on using 250-J of 1-micron laser light with 2-ns square pulses. Phase plates were employed giving a nominal spot diameter of 600-μm equivalent to an on-target irradiance of 4.5×10^{13} W/cm^2. Shocks were viewed edge-on in the disk (across the2-mm diameter). The molybdenum wires were overfilled with a 50-μm laser spot diameter giving a nominal irradiance of 2×10^{18} W/cm^2. The backlighter, shocked target and detector locations were set to try to optimize the phase contrast effects for a given x-ray energy and source size.

[a)]Contributed (or Invited) paper published as part of the Proceedings of the 18th Topical Conference on High-Temperature Plasma Diagnostics, Wildwood, New Jersey, May, 2010.

[b)]Author to whom correspondence should be addressed. Electonic mail: workman@lanl.gov

The relationship used to determine the optimal x-ray source to target distance is $z=(2\lambda u^2)^{-1}$, where z is the propagation distance, λ is the x-ray wavelength and u is the spatial frequency defined as the inverse of the x-ray source size in this context. Using an x-ray energy of 17.48-keV and an x-ray source size, defined by the wire

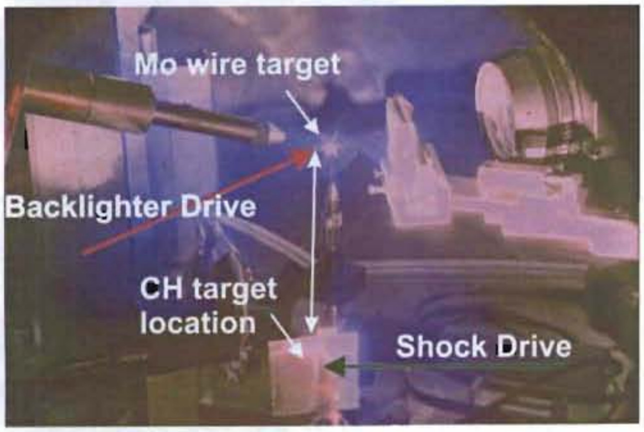

Figure 1 As shot target geometry showing backlighter position and polystyrene (CH) target location. The incident laser for the backlighter allowed the wire to be place tip-on to the target. The nanosecond shock drive is from the right. Backlighter and target are 25-cm apart while the detector is located 120-cm from the target.

diameter, of 12.5-µm the optimal distance from source to target is 110-cm (note this would be 17.6-cm for a 5-µm source). As shown in figure 1 target geometry drove the experiment to use a non-optimized distance of 25-cm between source and object. The detector plane was located at 120-cm beyond the target, giving a magnification of M=5.8. Image plates were used as the detection medium. The 2-ns shock drive entered the chamber on the right and irradiated the central portion of the polystyrene disk face. Data was collected on unshocked disks to determine spatial reference and uniformly showed stronger phase effects on the edges of the disks.

III. RESULTS

While experiments have been performed to characterize the x-ray source spatially, spectrally and under varying conditions this work concentrates on one image obtained under a phase-contrast geometry. Additional data was obtained at different x-ray energies and laser shock timing. Figure 2 shows an x-ray image taken at 17.48-keV using the emission from an end-on view of a molybdenum wire of diameter 12.5-µm and length 300-µm. The image is taken 4.3-ns after a shock is initiated from the right-hand side using a 2-ns laser drive as described previously. The x-ray energy has a very low absorption coefficient in the 2-mm polystyrene target (90% transmission) making the target itself difficult to see. One can see on the left edge of the target a white line running vertically. This is the effect of phase contrast at the very sharp density gradient from solid to vacuum. On the right hand side one can clearly see the shock generated in the

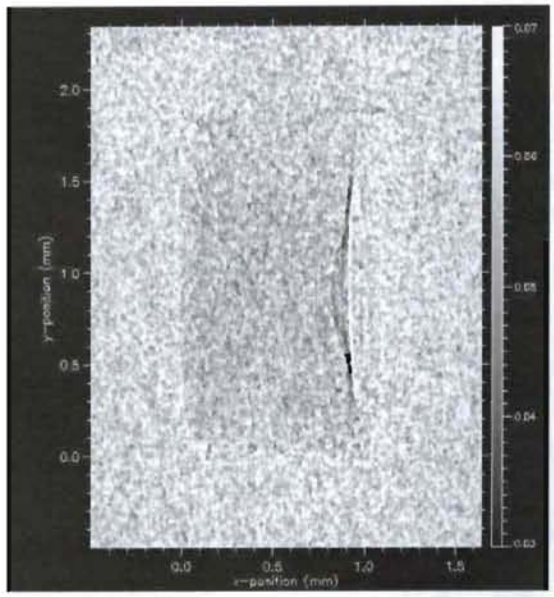

Figure 3Figure 2 X-ray image at 17.48-keV of a laser-shocked polystyrene disk observed at 4.3-ns after shock initiation. The shock drive proceeds from the right with a nominal spot diameter of 600-µm. The polystyrene disk is 2-mm in diameter and 1-mm thickness.

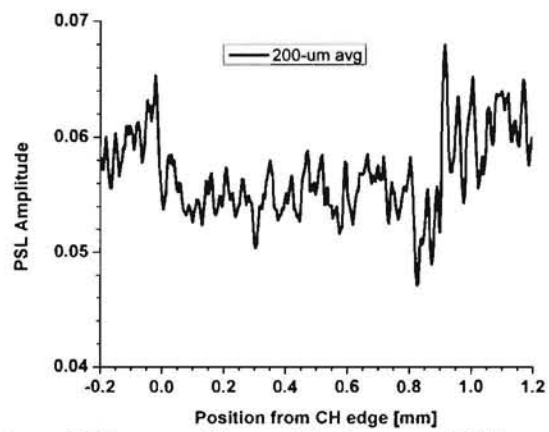

Figure 2 Lineout of figure 2 in the central 200-µm of the shocked region. Weak effects of phase contrast are seen as the occilitory intensity on the right side and far left side.

target that has propagated ~150-µm into the substrate. Recall that the shock drive initiates only in the central 600-µm of the 2-mm diameter disk and is why there appears to be a "bubble" moving in near the central region..The effects of phase contrast can be seen as light and dark bands in regions around the entire right side of the image. Figure 3 shows a lineout across a central 200-µm section of the shocked region. One can see the weak effects of the phase contrast imaging both on the left side (where the solid-vacuum interface exists) and the right side in the vicinity of the shock, near 0.9-mm. In this region the intensity profile oscillates as expected from the interference pattern produced in the phase contrast imaging. The background target signal is consistent with the 17.48-keV molybdenum x-ray source. While it seems clear when looking at the radiograph that phase contrast imaging is occurring it is clear from the lineout that the images are photon starved and suffering from significant background. While the image may not be sufficient to produce qualitative analysis of shock position it is a significant step forward in demonstrating this technique in a dynamic laser driven environment.

IV. HYDRO AND PHASE CALCULATIONS

In order to get a better feel for what is expected in a dynamic phase contrast image 1-D hydro calculations were performed and then post-processed to determine sensitivity to geometry. Figure 4 shows the results from a 1-D

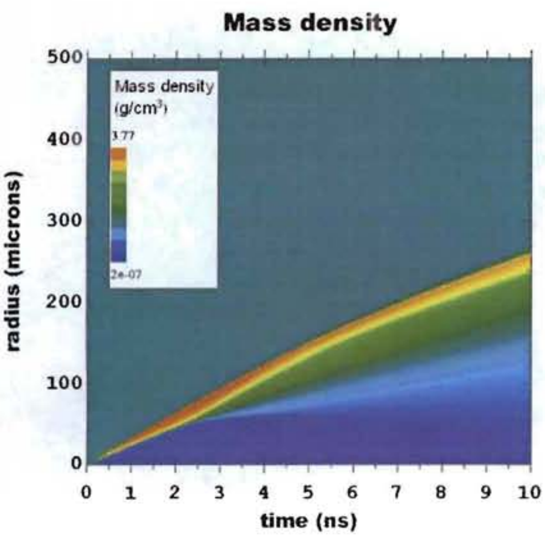

Figure 4 One-Dimensional Hydrodynamics calculation of a 2-ns laser drive with peak irradiance of 45-TW/cm^2 driving a polystyrene target.

hydrodynamics run using the HELIOS-CR code. A 2-ns laser drive was used with a peak irradiance of 45-TW/cm2. Data in the previous section was obtained at 4.3-ns. Data obtained at 6.3-ns shows the shock strength starting to dissipate.

Using the hydro calculation, a mass density profile was generated at 4.3-ns and then subsequently used to calculate the phase intensity produced at phase gradient locations. Figure 5 shows the mass density normalized to 1 (the actual mass density in solid polystyrene is 1.1 g/cc). Using a calculation developed by D. Montgomery et al [7] that solves the optical transfer function in Fourier space produces the expected intensity profiles due to phase

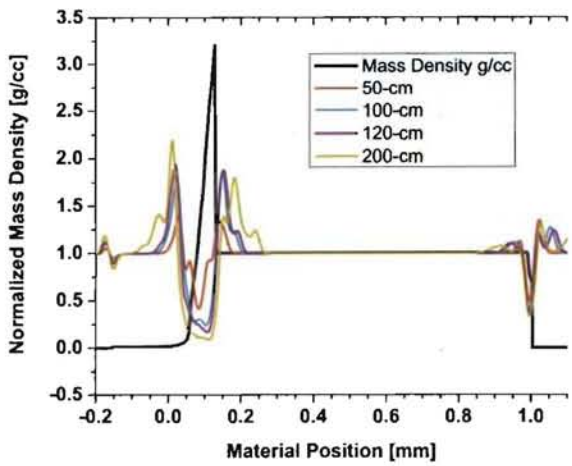

Figure 5 Normalized mass density profile and calculated phase intensity due to phase gradients in the mass profile as a function of x-ray propagation distance.

effects in a radiograph. Calculations use 17.48-keV with a source blurring factor (Gaussian) of 12-µm. The phase intensity is plotted as a function of distance from target object to detector. Two significant observation come from this figure. The first is the intensity of the phase effects increases with distance from the object to detector (this is up to some maximum not captured in the calculations). This is not surprising as the interference pattern created by the phase gradients change as a function of propagation distance. The second observation is the displacement of the phase profile with the position of the phase gradient (interface) producing it. This will significantly complicate the interpretation of radiographic data to determine interface positions in a purely phase driven radiograph.

While the radiograph is photon limited, the data suggests that the feasibility of using phase contrast imaging to view shocks in low density materials through a hohlraum environment may be possible. A good understanding of the phase gradients and x-ray optical transfer function is essential to interpret any interface locations.

V. ACKNOWLEGDEMENTS

The authors would like to thank the Trident laser crew and Ron Perea for target fabrication. This work was performed by Los Alamos National Laboratory under the auspices of the U. S. Department of Energy under contract No. DE-AC52-06NA25396.

---

[1] H.-S. Park, B.R. Maddox, E. Giraldez, S.P. Hatchett, L. T. Hudson, N. Izumi, M.H. Key, S.Le Pape, A.J. MacKinnon, A.G. MacPhee, P.K. Patel, T.W. Phillips, B.A. Remington, J.F. Seeley, R. Tommasini, R. Town, J.

Workman, E. Briambrink, Phys. Plasmas **15**, 072705 (2008).
[2] J. Workman, J. Cobble, K. Flippo, D.C. Gautier, S. LeztringRev. Sci. Instrum. **79** 10E905 (2008).
[3] E. Brambrink, H. G. Wei, B. Barbrel, P. Audebert, A. Benuzzi-Monaix, T. Boehly, T. Endo, C. Gregory, T. Kimura, R. Kodama, N. Ozaki, H.-S. Park, M. Rabec le Gloahec, M. Koenig Phys. Plasmas **16**, 033101 (2009).
[4] M.H. Key, M.D. Cable, T.E. Cowan, K.G. Estabrook, B.A. Hammel, S.P. Hatchett, E.A. Henry, D.E. Hinkel, J.D. Kilkenney, J.A. Koch, W.L. Kruer, A.B. Langdon, B.F. Lasinski, R.W. Lee, B.J. MacGowan, A. MacKinnon, J.D. Moody, M.J. Moran, A.A. Offenberger, D.M. Pennington, M.D. Perry, T.J. Phillips, T.C. Sangster, M.S. Singh, M.A. Stoyer, M. Tabak, G.L. Tietbohl, M. Tsukamoto, K. Wharton, S.C. Wilks Phys. Plasmas **5** 1966 (1998).
[5] A. Pogany, D. Gao, S.W. Wilkins Rev. Sci. Instum. **68** 2774 (1997).
[6] P. Cloetens, W. Ludwig, J. Baruchel, J-P Guigay, P. Pernot-Rejmankova, M. Salome-Pateyron, M. Schlenker, J-Y Buffiere, E. Marie, G. Peix J. Phys. D: Appl. Phys. **32** A145 (1999).
[7] D.S. Montgomery, A. Nobile, P.J. Walsh Rev. Sci. Instrum. **75** 3986 (2004).
[8] J. A. Koch, O.L. Landen, B. J. Kozioziemski, N. Izumi, E.L. Dewald, J.D. Salmonson, B.A. Hammel J. Appl. Phys. **105**, 113112 (2009).